J. Fluid Mech. (2001), *vol.* 445, *pp.* 305–325.
DOI: 10.1017/S0022112001005705 Printed in the United Kingdom

Compressible particle-driven gravity currents

By MARY-LOUISE E. TIMMERMANS, JOHN R. LISTER AND HERBERT E. HUPPERT

Institute of Theoretical Geophysics, Department of Applied Mathematics and Theoretical Physics, University of Cambridge, Silver Street, Cambridge CB3 9EW, UK

(Received 17 November 2000 and in revised form 5 May 2001)

Large-scale particle-driven gravity currents occur in the atmosphere, often in the form of pyroclastic flows that result from explosive volcanic eruptions. The behaviour of these gravity currents is analysed here and it is shown that compressibility can be important in flow of such particle-laden gases because the presence of particles greatly reduces the density scale height, so that variations in density due to compressibility are significant over the thickness of the flow. A shallow-water model of the flow is developed, which incorporates the contribution of particles to the density and thermodynamics of the flow. Analytical similarity solutions and numerical solutions of the model equations are derived. The gas–particle mixture decompresses upon gravitational collapse and such flows have faster propagation speeds than incompressible currents of the same dimensions. Once a compressible current has spread sufficiently that its thickness is less than the density scale height it can be treated as incompressible. A simple 'box-model' approximation is developed to determine the effects of particle settling. The major effect is that a small amount of particle settling increases the density scale height of the particle-laden mixture and leads to a more rapid decompression of the current.

1. Introduction

Particle-driven gravity currents are a form of buoyancy-driven flow that arises from a suspension of solid particles (for example, a silt-laden flow along the ocean floor or an avalanche). Large-scale particle-driven gravity currents occur in the atmosphere, for example, when a cold atmospheric flow passes over sandy or dusty land and entrains particles to form a severe dust storm, or as a result of explosive volcanic activity. During some explosive volcanic eruptions, a hot dispersion of gas and rock fragments is ejected from the vent of the volcano into the atmosphere and collapses to form a dense, laterally spreading pyroclastic flow. Pyroclastic flows can be up to several thousands of cubic kilometres in volume, propagating for tens of kilometres from the vent of a volcano at speeds over $200\,\mathrm{m\,s^{-1}}$ (Sparks *et al.* 1997).

Particle-driven gravity currents have been studied extensively, as reviewed by Simpson (1987) and Huppert (1998, 2000). Von Kármán (1940), and later Benjamin (1968), investigated theoretically the steady-state characteristics of an incompressible gravity current. In particular, they analysed the dynamics at the leading edge (or front) of a large Reynolds number gravity current of density ρ, propagating at constant speed over a horizontal surface into a quiescent surrounding fluid, of density ρ_a, as shown in figure 1. They found that the velocity u at the front of the current and the height h (away from the turbulent frontal region) are related by $u = Fr\,[(\rho - \rho_a)gh/\rho_a]^{1/2}$, where the dimensionless constant Fr is known as the Froude number. A relationship

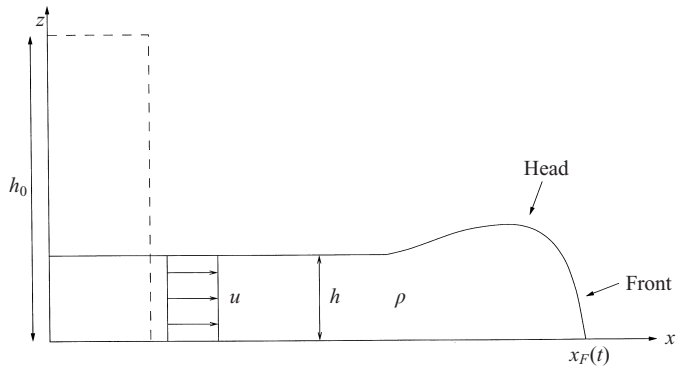

FIGURE 1. Schematic diagram of a gravity current of density ρ intruding at speed u into an infinitely deep body of surrounding fluid of smaller density. The dashed outline indicates the initial state (prior to collapse) of the gravity current.

of this form quantifies the resistance to the motion of the front due to the inertia of the surrounding fluid, viscous drag and turbulent Reynolds stress on the head of the current. Almost all subsequent theoretical studies of a gravity current on a solid boundary have used this front condition as a quasi-steady boundary condition to relate the speed $\mathrm{d}x_F(t)/\mathrm{d}t$ of the front at $x_F(t)$ to the height behind the front.

Bonnecaze, Huppert & Lister (1993) employed shallow-water theory to model the evolution from a state of rest of an incompressible particle-driven gravity current of fixed volume. Their study, which included comparisons with laboratory experiments, showed that the shallow-water equations, together with the front condition, accurately describe the flow evolution, including the settling of particles from the current as it propagates. Furthermore, Klemp, Rotunno & Skamarock (1994) employed a two-dimensional numerical model of a particle-free current to show that such shallow-water analyses capture the basic features that appear in the two-dimensional simulations. A simpler 'box-model' formulation, in which the current is assumed to evolve through a series of equal-area rectangles, has also been used to describe the basic properties of incompressible gravity currents (Huppert 1998, 2000). These horizontally averaged models often have the advantage of yielding solutions that can be expressed analytically in closed form. For example, Dade & Huppert (1996) constructed a box model to explain geological deposits from the Taupo volcano. They modelled the parent pyroclastic flow as a dilute, turbulent suspension and, through comparison with observational data, estimated an initial volume concentration of 0.3%.

Relatively few papers have considered the compressibility of a gas–particle gravity current. In order to understand the important problem of hazardous pyroclastic flows from explosive volcanic eruptions, models have been formulated to describe the fluid dynamics and thermodynamics of the gravitational collapse of an erupted volcanic mixture and the subsequent pyroclastic flow formation (Valentine & Wohletz 1989; Dobran & Neri 1993; Neri & Macedonio 1996). These complex numerical simulations are based on two-species turbulent-flow models and have a large number of adjustable parameters. In order to understand planetary-scale dust storms on Mars, Parsons (2000) describes them as compressible particle-driven gravity currents and argues that a plausible mechanism for the observed rapid growth of these flows is particle entrainment due to the passage of laterally propagating compressional shock waves. While we will show that a compressible current does not support

compressional shocks of this sort (contrast one-dimensional gas dynamics in shock tubes), our analysis provides an alternative explanation for these storms.

In incompressible analyses, the basic approximation applied is that the current is confined to a layer whose thickness is much less than its density scale height $\mathscr{H}_\rho$, defined as the typical value of $\rho/|\mathrm{d}\rho/\mathrm{d}z|$, where z denotes the vertical coordinate. Here, we show that the presence of particles in large-scale atmospheric gravity currents dramatically reduces the density scale height, so that variations in density due to compressibility are significant over the thickness of the flow. We analyse compressible currents within a similar framework to previous analyses of incompressible high Reynolds number gravity currents, in which the assumption is made that viscous forces are negligible and so the force balance is dominated by inertia and buoyancy. We use shallow-water theory to model an isentropic flow that originates from the instantaneous gravitational collapse of a fixed mass of gas and particles into lighter, infinitely deep surroundings. In addition, we investigate the effects of particle settling. We use parameter values typical of pyroclastic flows in order to illustrate the effects of compressibility. However, the equations and physical concepts presented here are also relevant to dust storms and provide a framework, for example, for modelling the rapid growth of dust storms on Mars.

This paper is organized as follows. The general properties (including assumptions) of the two-phase mixture are described in § 2, and we derive expressions for its temperature, pressure and density. In § 3, we consider flows with a constant mass fraction of particles and derive analytical similarity solutions as well as numerical solutions of the shallow-water equations, giving typical height and velocity profiles of a compressible particle-laden current. In § 4, we employ a box model to describe the effects of particle settling. We summarize our findings in the concluding section.

2. Thermodynamic properties of gas–particle mixtures

We make the following assumptions about the gas–particle mixture that forms the gravity current: (1) the particles are mono-disperse; (2) the mixture is dilute, so that interactions between the particles may be neglected and the pressure of the mixture is equal to that of the (ideal) gas phase alone; (3) vigorous turbulent mixing ensures that the particles are vertically well-mixed; and (4) the gas and particles are in thermal equilibrium.

We make assumption (1) for simplicity; the model could readily be modified to account for a polydisperse particle distribution (see, for example, Dade & Huppert 1996). Justification of assumptions (2) and (3) has been given by Dade & Huppert (1996), who modelled pyroclastic flows as low-concentration particle-driven gravity currents. Their box-model formulation was used together with observations of geological deposits to deduce that these deposits were formed by a dilute and highly turbulent flow. Assumption (4) can be justified for a powerful volcanic eruption, in which the mean diameter of the pyroclasts in the mixture is typically 1 mm or less (Woods 1995). Diffusion of heat through the solid particles determines the rate at which solid particles transfer their heat to the gas. This time is of order d^2/κ, where d is the particle diameter and $\kappa \approx 10^{-6}\,\mathrm{m^2\,s^{-1}}$ is the thermal diffusivity of the solid particle. Hence, particles less than 1 mm in diameter equilibrate thermally in less than a second, which is much shorter than the timescale $(h_0/g)^{1/2}$ for the current to propagate a distance equal to its initial height h_0.

The density ρ of a particle-driven gravity current can be expressed as a function of

the particle density ρ_p and the interstitial gas density ρ_g by

$$\frac{1}{\rho} = \frac{1-\phi}{\rho_g} + \frac{\phi}{\rho_p}, \tag{2.1}$$

where ϕ is the mass fraction occupied by the particles, which remains constant during any thermodynamic process. Since $\rho_p \gg \rho_g$, the mass fraction ϕ can be close to 1, even though the volume fraction $\phi\rho/\rho_p$ is assumed to be small.

In the following subsections, we derive relations for the temperature, pressure and density as functions of height in the gas–particle mixture.

2.1. *Equation of state*

We model the gas as ideal and thus the pressure, which is equal to that of the gas phase, is given by

$$p = \rho_g R T, \tag{2.2}$$

where T is the temperature, $R = c_p - c_v$ is a constant for any particular gas, equal to the universal gas constant divided by the molecular weight of the gas, and c_p and c_v are the specific heat capacities of the gas at constant pressure and volume respectively. Using (2.1), we can express the pressure as

$$p = \rho R_m T, \tag{2.3}$$

where $R_m = R(1-\phi)$ and we have neglected the volume of the particles (i.e. $\phi\rho/\rho_p \ll 1$). This is a reasonable assumption given the typical parameter values of a pyroclastic flow, $\rho_p = 2000\,\mathrm{kg\,m^{-3}}$, $\rho_g = 0.4\,\mathrm{kg\,m^{-3}}$ (at around 500 K) and $\phi = 0.96$ (Woods 1995). Equation (2.3) shows that the mixture of gas and particles behaves as an ideal 'pseudo gas' with a modified gas constant R_m (Wallis 1969).

2.2. *Vertical profile*

We assume that the pressure in the mixture varies hydrostatically with height z,

$$\frac{\mathrm{d}p}{\mathrm{d}z} = -\rho g. \tag{2.4}$$

The change in heat flow $\mathrm{d}Q$ between the system and its surroundings is given by the differential form of the First Law of Thermodynamics for a reversible process (Wood & Battino 1990),

$$\mathrm{d}Q = c_{pm}\mathrm{d}T - T\frac{\partial}{\partial T}\left(\frac{1}{\rho}\right)_p \mathrm{d}p, \tag{2.5}$$

where c_{pm} is the specific heat capacity of the mixture at constant pressure. Similarly, let c_{vm} denote the specific heat capacity at constant volume. The specific heat capacities of the mixture are given by

$$c_{pm} = \phi c + (1-\phi)c_p \quad \text{and} \quad c_{vm} = \phi c + (1-\phi)c_v, \tag{2.6a,b}$$

where c is the specific heat of the incompressible solid particles, for which the specific heats at constant volume and constant pressure can be taken to be equal (Bohren & Albrecht 1998). All heat capacities are assumed to be constant.

We take $\mathrm{d}Q = 0$ under the assumption that the timescale of thermal diffusion over the current is considerably longer than the timescale of fluid motion in the current (i.e. the flow is adiabatic). Hence, we couple (2.1), (2.2) and (2.5) to deduce that

$$c_{pm}\,\mathrm{d}T = \frac{(1-\phi)}{\rho_g}\,\mathrm{d}p. \tag{2.7}$$

Recall that we are assuming a sufficiently vigorous flow that turbulent mixing maintains a vertically uniform particle mass fraction ϕ. We use (2.7) with (2.4) to deduce that the vertical temperature gradient in the mixture is constant,

$$\frac{\mathrm{d}T}{\mathrm{d}z} = -\frac{g}{c_{pm}}, \tag{2.8}$$

where again we have neglected the volume of the particles. We solve (2.8) to obtain the temperature profile

$$T(x,z,t) = T_i\left[1 + \frac{(h-z)}{\mathscr{H}}\right], \tag{2.9}$$

where T_i is the temperature at the top of the current ($z = h$) and $\mathscr{H} = c_{pm}T_i/g$ has the dimensions of length. To a good approximation for our applications, we take $c_{pm} \approx c_p$, a constant (i.e. $\mathscr{H} = c_pT_i/g$) (Woods 1988). This does not change the value of R_m.

We couple (2.2) with (2.7) to obtain the isentropic relations,

$$\frac{T}{T_i} = \left(\frac{p}{p_a}\right)^{(\gamma-1)/\gamma} = \left(\frac{\rho_g}{\rho_{gi}}\right)^{\gamma-1}, \tag{2.10a,b}$$

where $\gamma = c_{pm}/c_{vm}$ is the isentropic exponent of the mixture and ρ_{gi} is the density of the gas at $z = h$. We substitute (2.9) into (2.10*a*) and (2.10*b*) to find the pressure and the density of the mixture,

$$p(x,z,t) = p_a\left[1 + \frac{(h-z)}{\mathscr{H}}\right]^{\gamma/(\gamma-1)} \tag{2.11}$$

$$\rho(x,z,t) = \rho_i\left[1 + \frac{(h-z)}{\mathscr{H}}\right]^{1/(\gamma-1)}, \tag{2.12}$$

where p_a is the ambient pressure and $\rho_i = \rho_{gi}/(1-\phi)$ is the density of the mixture at $z = h$.

2.3. *Density scale height*

In a hydrostatic pressure field, density changes become important over a height $\rho/|\mathrm{d}\rho/\mathrm{d}z|$. Hence, using (2.12), we define the density scale height by

$$\mathscr{H}_\rho = \mathscr{H}(\gamma-1) = \frac{\gamma R(1-\phi)T_i}{g} = \frac{\gamma p_a}{\rho_i g}. \tag{2.13}$$

Thus, compressibility effects are important in a current of height h when $h/\mathscr{H}_\rho \gtrsim O(1)$. The density scale height of an adiabatic atmosphere of the same temperature but without particles is given by $\mathscr{H}_s = \mathscr{H}(\gamma_g - 1) = \gamma_g RT_i/g$, where $\gamma_g = c_p/c_v$ is the isentropic exponent of the pure gas. Hence, $\mathscr{H}_\rho \ll \mathscr{H}_s$ because $(1-\phi) \ll 1$ for the mass fractions common in the flows that we are considering (i.e. the presence of particles greatly reduces the scale height).

We present typical parameter values for a pyroclastic flow mixture in table 1. The gas phase in some pyroclastic flows is predominantly water vapour for which $\gamma_g \approx 1.26$ (Kieffer 1984), whereas the Earth's atmosphere has $\gamma_g \approx 1.4$ (Gill 1982). These variations are relatively unimportant when particles are present (Kieffer 1984). The isentropic exponent γ of the mixture takes values between $\gamma = \gamma_g$ (corresponding to $\phi = 0$) and $\gamma = 1$ (corresponding to $\phi = 1$). The density scale height for a typical

Initial mass fraction of particles	ϕ_0	0.96
Particle density	ρ_p	$2000\,\mathrm{kg\,m^{-3}}$
Initial height	h_0	1 km
Initial temperature at the top	T_{i0}	500 K
Particle settling velocity	v_s	$0.5\,\mathrm{m\,s^{-1}}$
Gas constant	R	$462\,\mathrm{J\,K^{-1}\,kg^{-1}}$
Specific heat at constant pressure of the gas	c_p	$1600\,\mathrm{J\,K^{-1}\,kg^{-1}}$
Specific heat of the solid particles (pyroclasts)	c	$1600\,\mathrm{J\,K^{-1}\,kg^{-1}}$
Isentropic exponent of the gas	γ_g	1.4

TABLE 1. Two-phase mixture conditions of gas and particles in the pyroclastic flow. Typical values are taken from Woods (1995) and Dade & Huppert (1996).

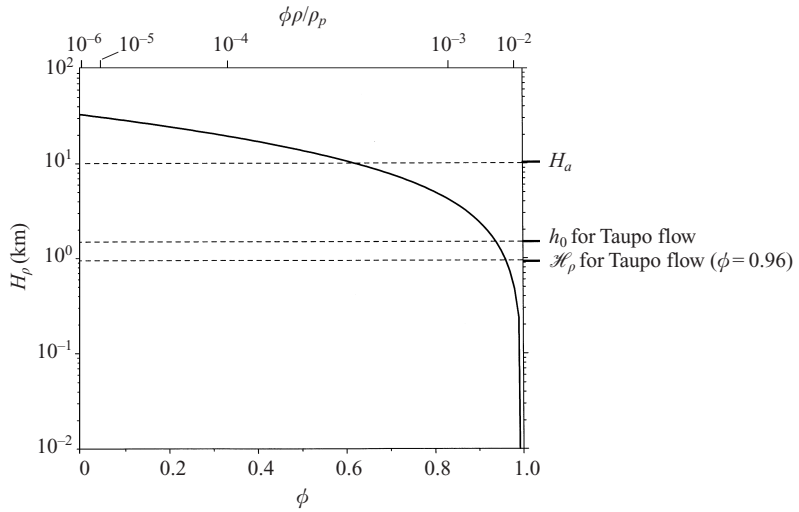

FIGURE 2. Density scale height of a pyroclastic flow as a function of particle mass fraction, calculated for the typical values in table 1. Estimates of h_0 and $\mathscr{H}_\rho$ for the Taupo pyroclastic flow from the 180 AD Taupo eruption in New Zealand are taken from Dade & Huppert (1996). The volume fractions $\phi\rho/\rho_p$, calculated with $\rho_g = 0.4\,\mathrm{kg\,m^{-3}}$, are small even when the mass fraction ϕ reaches 0.99.

pyroclastic flow is shown in figure 2 as a function of particle mass fraction. For large particle mass fractions, $\mathscr{H}_\rho \ll \mathscr{H}_a \approx 10$ km (Gill 1982), where $\mathscr{H}_a$ is the density scale height of the atmosphere.

2.4. *A stationary vertical column in the atmosphere*

Consider a stationary vertical column of height h of a fixed mass of a gas–particle mixture in the atmosphere, with temperature, pressure and density profiles given by (2.9), (2.11) and (2.12), and assume a hydrostatic pressure distribution in the surrounding motionless atmosphere. Furthermore, variations in ρ_a are only significant over heights comparable to $\mathscr{H}_a$. For simplicity, we make the assumption, appropriate for typical heights of particle-driven flows in the atmosphere, that $h \ll \mathscr{H}_a$ and hence we take ρ_a to be uniform. The pressure p_a at the top of the particle-laden column is then given by $p_a = p_0 - \rho_a g h$, where p_0 is the atmospheric pressure at ground level ($z = 0$). Furthermore, for the heights that we are considering, $p_a \gg \rho_a g h$ (we take $p_0 = 10^5\,\mathrm{Pa}$ and $\rho_a = 1.2\,\mathrm{kg\,m^{-3}}$) and hence we make the approximation throughout

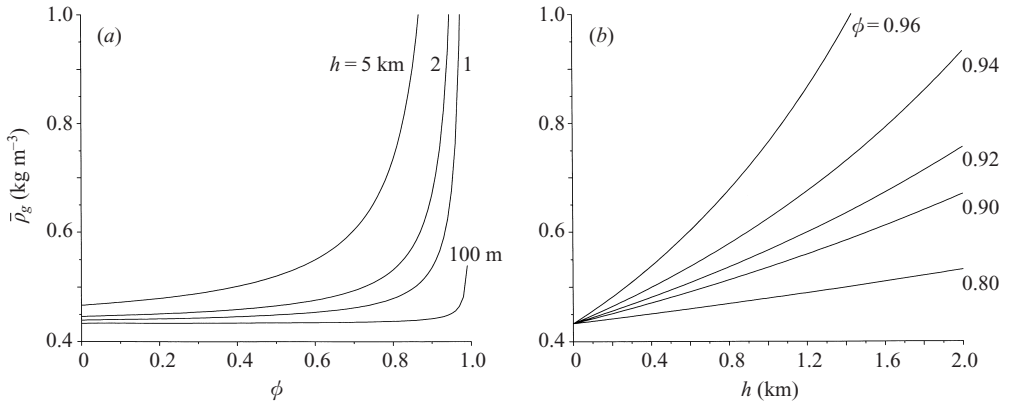

FIGURE 3. (*a*) $\bar{\rho}_g$ as a function of ϕ, in columns of height 5 km, 2 km, 1 km and 100 m. (*b*) $\bar{\rho}_g$ as a function of h, in columns with different particle mass fractions. All curves have $p_a = 10^5$ Pa.

that $p_a = p_0$, a constant. Finally, by continuity of pressure at the top of the column, $p_a = \rho_{gi} R T_i$, which couples the values of ρ_{gi} and T_i to p_a. This implies that ρ_{gi}, T_i and $\mathscr{H}$ are also constant.

It is instructive to examine how the density varies both as a function of the particle mass fraction, and between columns of different heights. We introduce the height-averaged density,

$$\bar{\rho} \equiv \frac{1}{h}\int_0^h \rho \, \mathrm{d}z = \frac{p_a}{gh}\left[\left(1 + \frac{h}{\mathscr{H}}\right)^{\gamma/(\gamma-1)} - 1\right], \tag{2.14a,b}$$

and the height-averaged gas density is then given by $\bar{\rho}_g = \bar{\rho}(1-\phi)$. Figure 3 shows the dependence of $\bar{\rho}_g$ on the particle mass fraction for columns of different heights and on column height for mixtures having different particle mass fractions.

The important parameters that influence the gas density in the column are h, T_i and ϕ (which determines γ). These parameters determine the ratio $h/\mathscr{H}_\rho$ and hence the importance of compressibility effects. As the mass loading becomes large ($\phi \to 1$), the exponent in (2.14) becomes large since, as is readily shown from (2.6),

$$\frac{\gamma}{\gamma - 1} = \frac{\gamma_g}{\gamma_g - 1} + \frac{\phi}{1-\phi}\frac{c}{R}. \tag{2.15}$$

Large variations in the gas density occur in this case because the mixture has the compressibility of the gas, but with a much higher density due to the presence of the solid particles. The large density leads to a large variation in the hydrostatic pressure over the height of the column. We refer to the isentropic relations (2.10) to remark that, since the pressure in the flow decreases rapidly for small decreases in particle mass fraction, the density likewise decreases rapidly, while the temperature remains nearly uniform. Thus, the solid particles have a buffering effect; they act as a heat source for the expanding gas and so the temperature hardly changes.

3. Shallow-water theory without particle settling

In this section, we present analytical and numerical solutions for a current when there is neither gravitational particle settling nor entrainment of particles ($\phi = \phi_0$, a constant). This corresponds, for example, to the early evolution of a current with

$v_s \ll \sqrt{gh_0}$, where v_s is the settling speed of the particles. Thus, the current has to propagate many times its height before particle settling becomes significant.

3.1. *Shallow-water equations*

We consider a two-dimensional current of density $\rho(x,z,t)$ created by the instantaneous release from rest of a fixed mass of a gas–particle mixture into a calm surrounding atmosphere. The model can be extended to describe continuous release or an axisymmetric flow in a similar manner to the incompressible case (Bonnecaze *et al.* 1995). The high Reynolds number gravity current propagates under a balance of inertial and buoyancy forces over a rigid, horizontal surface under an infinitely high, incompressible, lighter layer of uniform density, as sketched in figure 1. For the two-dimensional flow field $\boldsymbol{u} = (u,w)$, the inviscid equations of motion are

$$\frac{\mathrm{D}\rho}{\mathrm{D}t} + \rho\left(\frac{\partial u}{\partial x} + \frac{\partial w}{\partial z}\right) = 0, \tag{3.1}$$

$$\rho\frac{\mathrm{D}u}{\mathrm{D}t} + \frac{\partial p}{\partial x} = 0, \tag{3.2}$$

$$\rho\frac{\mathrm{D}w}{\mathrm{D}t} + \frac{\partial p}{\partial z} + \rho g = 0, \tag{3.3}$$

where x and z are the horizontal and vertical coordinates and p is the pressure.

Soon after the stationary gas–particle mixture collapses, it quickly spreads so that its characteristic horizontal lengthscale L is much greater than its characteristic thickness H. As we shall see, the characteristic horizontal velocity is $(gH)^{1/2}$ and hence, by continuity, the characteristic vertical velocity is $(H/L)(gH)^{1/2}$. From (2.13) the speed of sound in the mixture is of order $(g\mathscr{H}_\rho)^{1/2}$. We consider the case $H = O(\mathscr{H}_\rho)$, in which compressibility affects the horizontal propagation, but $(H/L)^2 H \ll \mathscr{H}_\rho$ so that hydrostatic equilibrium can be established in each vertical column on a shorter timescale than propagation of the current. Equation (3.3) reduces to

$$\frac{\partial p}{\partial z} + \rho g = 0, \tag{3.4}$$

and we can use the results of § 2.2 to describe the vertical pressure and density profiles.

Once the current has spread sufficiently that its height $h(x,t)$ varies only slowly over the horizontal distance x (i.e. $\partial h/\partial x \ll 1$), following Bonnecaze *et al.* (1993), the overall behaviour of the flow can be studied by neglecting the variation of the horizontal velocity over the height of the current. We assume that vigorous turbulent motion ensures that horizontal momentum is vertically well-mixed, in the same way that it ensures a vertically uniform particle concentration. With these assumptions, we replace the velocity by its average value $u(x,t)$ over the height of the current. Such a simplification is valid when there are no abrupt variations in the height; clearly, it will not hold in the immediate vicinity of the front.

The approximation that u is independent of z allows us to integrate the governing equations over the height of the current. We use (2.14) to express the height-integrated continuity and horizontal-momentum equations as

$$\frac{\partial}{\partial t}(\bar{\rho}h) + \frac{\partial}{\partial x}(\bar{\rho}uh) = 0, \tag{3.5}$$

$$\frac{\partial}{\partial t}(\bar{\rho}uh) + \frac{\partial}{\partial x}(\bar{\rho}u^2h) + \frac{\partial}{\partial x}(\bar{p}h - p_a h) = 0, \tag{3.6}$$

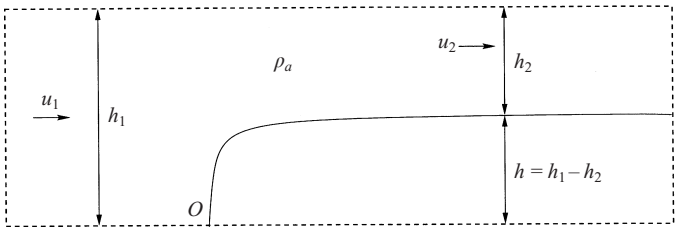

FIGURE 4. Steady flow past a stationary wedge of fluid of constant density.

where $\bar{p} = (\int_0^h p\,\mathrm{d}z)/h$. Alternatively, we can express (3.6) in terms of the height-averaged density by

$$\frac{\partial}{\partial t}(\bar{\rho}uh) + \frac{\partial}{\partial x}\left(\bar{\rho}u^2h + \frac{\gamma-1}{2\gamma-1}\bar{\rho}gh\mathscr{H}\left(1+\frac{h}{\mathscr{H}}\right) - \frac{\gamma}{2\gamma-1}p_ah\right) = 0. \tag{3.7}$$

We note that the shallow-water equations for an incompressible gravity current, as given by Bonnecaze *et al.* (1993), can be recovered by taking the limit $h/\mathscr{H}_\rho \to 0$ of these equations.

3.2. *The front condition*

Here, we consider the steady gravity-driven flow of a compressible gas–particle mixture and employ a technique similar to that of Benjamin (1968) to derive a moving boundary condition (a front condition) at $x = x_F(t)$, which is required for closure to the shallow-water equations. We consider a wedge of a stationary gas–particle mixture in a frame of reference moving with the current and balance the flow force (the momentum fluxes plus the pressure forces) between upstream and downstream regions in a control volume of the surrounding steady flow, as shown in figure 4. The fluid overlying the stationary wedge is incompressible, with a uniform density ρ_a, and the pressure variation with height is hydrostatic at upstream and downstream cross-sections. The height and the flow speed are constant far upstream and we assume that the flow speed is constant downstream.

We couple the momentum-integral theorem and conservation of mass. Then, assuming no energy loss, application of Bernoulli's theorem along the free surface of the wedge between the stagnation point O and the downstream cross-section, indicates that the front condition is given by

$$u = Fr[(\bar{\rho}-\rho_a)gh/\rho_a]^{1/2} \quad (x = x_F(t)), \tag{3.8}$$

where $Fr = \sqrt{2}$. This reduces to the result found by Benjamin (1968) in the incompressible limit $h/\mathscr{H}_\rho \to 0$. The Froude number has a theoretical value of $\sqrt{2}$ for an energy-conserving flow. However, viscous drag and turbulent Reynolds stresses result in additional momentum loss at the front of a real current, yielding a slower flow; Huppert & Simpson (1980) established the experimental value $Fr = 1.19$.

The derivation of (3.8) is based on a motion driven by gravity and resisted by the inertia of the surrounding fluid (i.e. external drag), in which the inertia of the moving layer plays no role since the frontal wedge is stagnant in the moving frame of reference. For a typical pyroclastic flow, $\bar{\rho}/\rho_a \approx 16$ (cf. the parameters given in table 1 with $\rho_a = 1.2\,\mathrm{kg\,m^{-3}}$ at $10\,^\circ\mathrm{C}$). For these large density ratios, it seems likely that the inertia and Reynolds stresses in the heavier fluid play a significant role and hence that the Froude number will be some function of the density ratio between the two fluids. This function must be determined experimentally (or numerically). See,

for example, Grobelbauer, Fannelop & Britter (1993). In our modelling of pyroclastic flows, we write the front condition as

$$u = Fr[(\bar{\rho} - \rho_a)gh/\bar{\rho}]^{1/2} \quad (x = x_F(t)), \tag{3.9}$$

where Fr may still be a function of $\bar{\rho}/\rho_a$, but is expected to be $O(1)$ for both small and large density ratios. We take $Fr = 1.19$ in the numerical results.

In this shallow-water analysis, we consider only currents that have large mass fractions $\phi \approx 1$ and $\rho_a/\bar{\rho} \ll 1$; hence, we neglect ρ_a and replace (3.9) by

$$u = Fr(gh)^{1/2} \quad (x = x_F(t)). \tag{3.10}$$

Numerical solutions may be obtained to the full problem in which neither the atmospheric density nor the variation of interfacial quantities with height are neglected. However, the algebra is considerably more complex and the equations do not admit analytical solutions. Hence, we restrict our shallow-water analysis to the case described above.

3.3. *Non-dimensionalization*

It is convenient to non-dimensionalize the shallow-water equations and boundary conditions using initial parameters of the current. We non-dimensionalize lengths by the initial height of the current h_0, time by $(h_0/g)^{1/2}$, velocity by $(gh_0)^{1/2}$ and density by ρ_i. The resulting dimensionless shallow-water equations and boundary conditions are given by

$$\frac{\partial}{\partial t}(\bar{\rho}h) + \frac{\partial}{\partial x}(\bar{\rho}uh) = 0, \tag{3.11}$$

$$\frac{\partial}{\partial t}(\bar{\rho}uh) + \frac{\partial}{\partial x}\left(\bar{\rho}u^2h + \frac{\gamma - 1}{2\gamma - 1}\frac{\bar{\rho}h\mathscr{H}}{h_0}\left(1 + \frac{h_0 h}{\mathscr{H}}\right) - \frac{\gamma - 1}{2\gamma - 1}\frac{h\,\mathscr{H}}{h_0}\right) = 0, \tag{3.12}$$

$$u = 0 \qquad (x = 0), \tag{3.13}$$

$$u = Fr\sqrt{h} \qquad (x = x_F(t)), \tag{3.14}$$

where

$$\bar{\rho}h = \frac{\mathscr{H}}{h_0}\frac{\gamma - 1}{\gamma}\left[(1 + h_0 h/\mathscr{H})^{\gamma/(\gamma-1)} - 1\right] \tag{3.15}$$

and all variables are now dimensionless. The dimensionless system depends on Fr and two parameters, $h_0/\mathscr{H}$ and γ, that describe the effects of compressibility. Finally, we consider a current that is formed by the release of a fixed mass of fluid plus particles. The total mass per unit width of the current is given by

$$m = \int_0^{x_F(t)} \bar{\rho}h \,\mathrm{d}x. \tag{3.16}$$

If there is no entrainment and no particle loss then m is constant, while $m = m(\phi)$ otherwise.

3.4. *Analytical similarity solutions*

The effects of compressibility are important if $h_0 h/\mathscr{H}_\rho \gg 1$, which requires $\gamma - 1 \ll 1$ or $h_0 h/\mathscr{H} \gg 1$. If $h_0 h/\mathscr{H} = O(1)$ while $\gamma - 1 \to 0$, which is the case of practical significance for pyroclastic flows, then it is apparent from the limit of (3.15) that there is no similarity solution to the governing equations (3.11)–(3.16). However, in

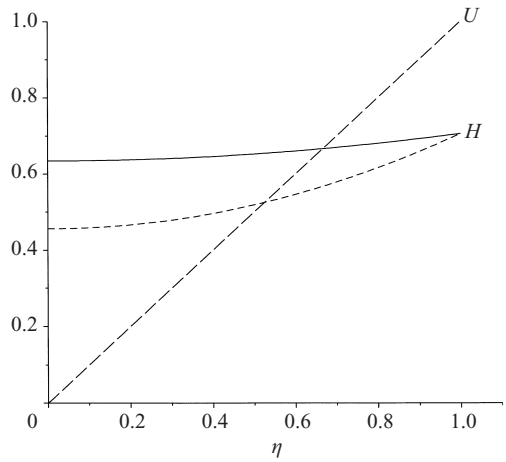

FIGURE 5. Self-similar solutions for velocity $U(\eta)$ and height $H(\eta)$ with $\gamma = 1.4$ and $Fr = 1.19$. The solid curve shows $H(\eta)$ for $h_0 h/\mathscr{H}_\rho \gg 1$; the dashed curve shows $H(\eta)$ for $h_0 h/\mathscr{H}_\rho \ll 1$. The velocity $U(\eta)$ (long-dashed) is the same in both limits.

the limit $h_0 h/\mathscr{H}_\rho \gg 1$ with $\gamma - 1 = O(1)$ (3.11) and (3.12) become

$$\frac{\partial}{\partial t}(h^{\gamma/(\gamma-1)}) + \frac{\partial}{\partial x}(uh^{\gamma/(\gamma-1)}) = 0, \tag{3.17}$$

$$\frac{\partial}{\partial t}(uh^{\gamma/(\gamma-1)}) + \frac{\partial}{\partial x}\left(u^2 h^{\gamma/(\gamma-1)} + \frac{\gamma-1}{2\gamma-1} hh^{\gamma/(\gamma-1)}\right) = 0. \tag{3.18}$$

Estimates of the terms in (3.17) and (3.18) suggest the order-of-magnitude scalings

$$u \sim \frac{x}{t}, \quad h \sim u^2 \quad \text{and} \quad h^{\gamma/(\gamma-1)} x \sim \tilde{m}, \tag{3.19}$$

where $\tilde{m} = m[\gamma/(\gamma-1)](\mathscr{H}/h_0)^{1/(\gamma-1)}$ and the last balance has been deduced from the limiting form of (3.16). These balances are the basis for a similarity solution

$$u(x,t) = \dot{x}_F(t) U(\eta), \qquad h(x,t) = [\dot{x}_F(t)]^2 H(\eta), \tag{3.20}$$

where

$$\left.\begin{aligned} &\eta = x/x_F(t), \quad H(\eta) = \frac{\gamma-1}{4\gamma}(\eta^2 - 1) + \frac{1}{Fr^2}, \quad U(\eta) = \eta, \\ &x_F(t) = \left[\tilde{m}^{\gamma-1}\left(\frac{3\gamma-1}{2\gamma}\right)^{2\gamma}\left(\int_0^1 H^{\gamma/(\gamma-1)}\,\mathrm{d}\eta\right)^{1-\gamma}\right]^{1/(3\gamma-1)} t^{2\gamma/(3\gamma-1)}. \end{aligned}\right\} \tag{3.21}$$

This solution will cease to hold when h has decreased sufficiently that $hh_0/\mathscr{H}_\rho \sim 1$. From (3.20) and (3.21), this is when $t \sim (h_0/\mathscr{H}_\rho)^{(3\gamma-1)/(2\gamma-2)}$.

In the limit $h_0 h/\mathscr{H}_\rho \to 0$, equations (3.11) and (3.12) also possess a similarity solution, given by (3.20), where now

$$U(\eta) = \eta, \quad H(\eta) = \tfrac{1}{4}(\eta^2 - 1) + \frac{1}{Fr^2}, \quad x_F(t) = \left[\frac{27 Fr^2 x_0}{(12 - 2Fr^2)}\right]^{1/3} t^{2/3}, \tag{3.22}$$

and x_0 is the dimensionless fixed volume of the current. This is the incompressible shallow-water similarity solution given by Bonnecaze *et al.* (1993).

Figure 5 shows the self-similar velocity and height profiles in the two limits

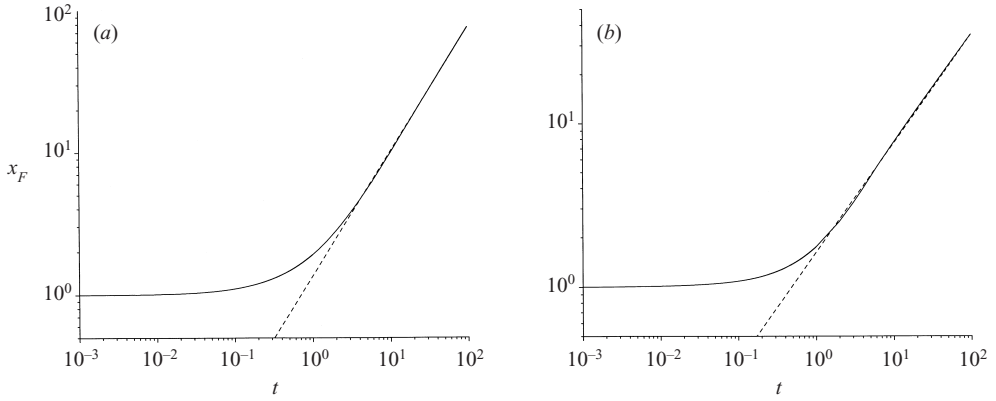

FIGURE 6. Frontal position x_F as a function of time for (*a*) $h_0/\mathscr{H}_\rho = 250$ and $\gamma = 1.4$ and (*b*) $h_0/\mathscr{H}_\rho = 2.5 \times 10^{-3}$ and $\gamma = 1.4$. In (*a*) the full numerical solution (solid curve) asymptotes to the form $x_F \propto t^{2\gamma/(3\gamma-1)}$ (dashed line), indicating the long-time self-similar behaviour (cf. (3.21)); while in (*b*) the full numerical solution (solid curve) asymptotes to the form $x_F \propto t^{2/3}$ (dashed line), indicating the long-time self-similar behaviour (cf. (3.22)). The currents have initial length equal to the initial height.

$h_0h/\mathscr{H}_\rho \gg 1$ with $\gamma - 1 = O(1)$, and $h_0h/\mathscr{H}_\rho \ll 1$. The height profiles change abruptly at $\eta = 1$ due to the front condition. The velocity profile is the same in both limits; it increases linearly from $U(0) = 0$ at the tail of the current to $U(1) = 1$ at the front. In both limits, the height increases quadratically towards the front. This increase contributes to a horizontal pressure gradient over the length of the current, with the largest pressure at the front, resulting in a deceleration behind the front. The increase in height towards the front is not as pronounced for the compressible current, which decompresses and expands laterally as it lengthens and thins, yielding a more uniform height over its length.

3.5. *Numerical results*

When $h_0h/\mathscr{H}_\rho = O(1)$, there are no analytical solutions to (3.11)–(3.14) and we obtain numerical solutions using the method described in the Appendix. Figure 6 plots the numerical and similarity solutions for compressible ($h_0h/\mathscr{H}_\rho \gg 1$) and incompressible ($h_0h/\mathscr{H}_\rho \ll 1$) currents. In the initial phase of the current, the mixture collapses and approaches its self-similar form, which it attains before $t = 10$. The subsequent self-similar propagation depends on the initial mass or volume of the current, but not on the initial aspect ratio or velocity, as is evident from the form of (3.21) and (3.22).

Height profiles for compressible gravity currents are shown in figure 7. The fixed-mass currents start from rest with initial lengths equal to their starting heights. The currents collapse, lengthen and thin, ultimately assuming the self-similar form for $h_0h/\mathscr{H}_\rho \ll 1$. The profiles in figure 7(*a*) correspond to a particle-free current with an initial height of 100 m (all other parameters are given in table 1). This is essentially an incompressible current; it has a large density scale height that is not reduced by the presence of particles, and an initial height that is much less than this density scale height. The results are indistinguishable from those computed using an incompressible model. The profiles in figure 7(*b*) correspond to a current with a mass fraction $\phi_0 = 0.96$ (scale height $\mathscr{H}_\rho$ about 1 km) and an initial height h_0 of about 1 km. Compressible effects play an observable role in this case because the current has

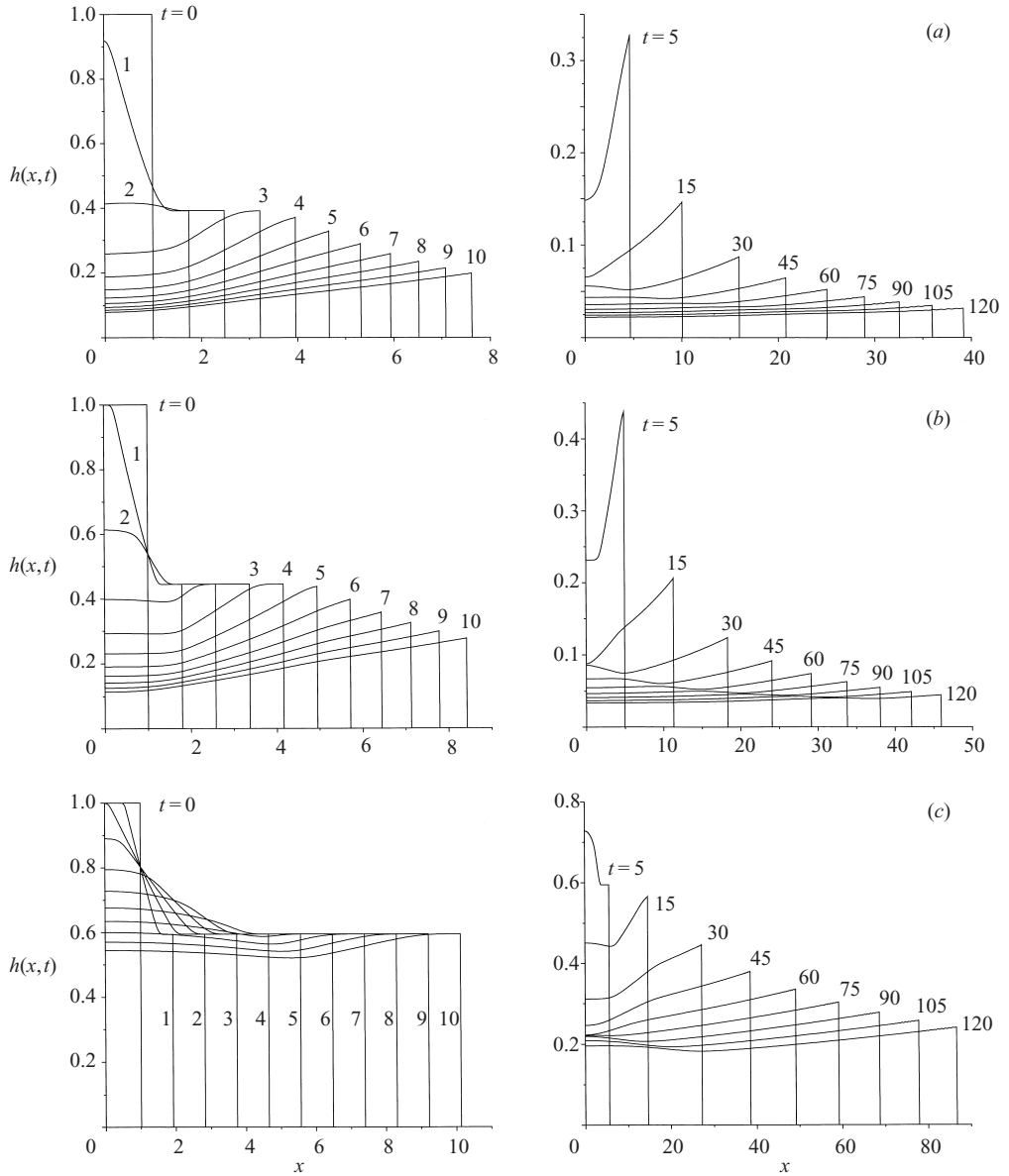

FIGURE 7. Numerically determined height $h(x,t)$ profiles of a collapsing gravity current with (*a*) $h_0/\mathscr{H}_\rho = 3 \times 10^{-3}$, $\gamma = 1.4$, (*b*) $h_0/\mathscr{H} = 0.012$ and $\phi_0 = 0.96$ ($h_0/\mathscr{H}_\rho \approx 1$ and $\gamma \approx 1.01$) and (*c*) $h_0/\mathscr{H} = 0.06$ and $\phi_0 = 0.96$ ($h_0/\mathscr{H}_\rho \approx 5$ and $\gamma \approx 1.01$). The left-hand panels show early times and the right-hand panels later times. The more compressible currents, (*b*) and (*c*), expand and propagate faster in dimensionless variables than the almost incompressible current (*a*). (Dimensional velocities are proportional to $(gh_0)^{1/2}$.)

a larger initial height than the current of figure 7(*a*), combined with a smaller density scale height caused by a large particle mass fraction. The overall structure of this current is similar to that of the incompressible current with the main distinguishing feature being an initial decompression (and associated volume expansion) upon collapse of the compressible current. This can be seen in the difference in height

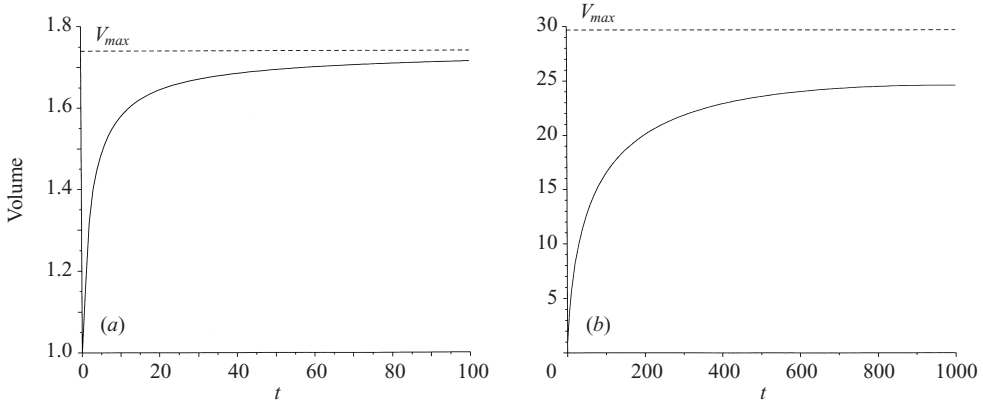

FIGURE 8. Volume as a function of time for: (*a*) the current in figure 7(*b*); and (*b*) the current in figure 7(*c*).

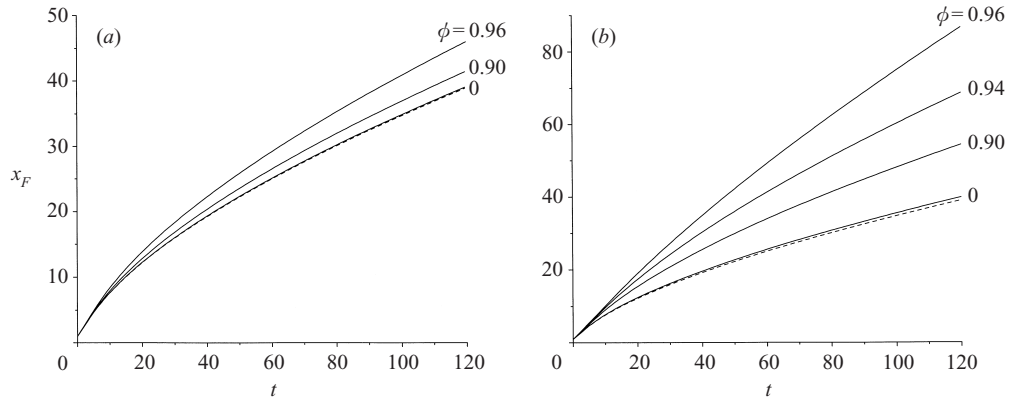

FIGURE 9. x_F as a function of time for currents having different particle mass fractions ϕ, and hence different values of γ. The dashed curve is for an incompressible current. (*a*) $h_0/\mathscr{H} = 0.012$ and (*b*) $h_0/\mathscr{H} = 0.06$. The currents propagate more rapidly for larger values of $h_0/\mathscr{H}_\rho$ due to decompression.

profiles between the two currents at early times ($t = 2, 3$). The profiles in figure 7(*c*) correspond to a current with $\phi_0 = 0.96$ and a rather large initial height ($h_0 = 5\,\mathrm{km}$). The volume expansion is now clearly evident by comparison of these profiles to the profiles of the incompressible current. The compressible currents decompress as they lengthen and thin, with the most rapid decompression occurring just after release of the mixture, when the most rapid thinning occurs. The density of the fixed mass mixture decreases as it decompresses and expands.

Figure 8 shows the volume expansion as a function of time for the currents in figure 7(*b*, *c*). The mixture decompresses to a maximum volume $V_{max} = m/\lim_{h\to 0}\bar{\rho}$ as the density decreases to that of the mixture at atmospheric pressure. The decompression takes longer for the current with the larger initial height (figure 8*b*).

Figure 9 shows the front position as a function of time for currents having different particle mass fractions for two values of $h_0/\mathscr{H}$. The curves show that the frontal speed is larger for a current with a larger particle mass fraction at a given ratio of its initial height relative to its density scale height in the absence of particles. The frontal

speed is largest for a current having a high mass fraction of particles and a large initial height relative to its density scale height in the absence of particles. Hence, the curves show that a compressible current propagates faster than an incompressible current for the same initial height. This is because the internal energy of compression is released upon decompression and transformed into kinetic energy of motion. The faster front speed of a compressible current can also be explained in terms of forces: the expansion results in a less rapid thinning (than an incompressible current) and maintains a larger driving pressure gradient $\partial(\bar{p}h)/\partial x$.

4. The effects of particle settling

Particle-settling currents are more complex than their non-settling counterparts because decreases in the particle mass fraction due to settling over time alter the thermodynamic properties, and hence the driving buoyancy force, in a manner that is not straightforward. We do not attempt to solve the full shallow-water equations numerically, but rather we employ a simpler model that captures the essential physical processes. Furthermore, we show that a full numerical solution of a settling, compressible gravity current is unnecessary because particle settling influences the flow dynamics only after the current has attained its self-similar form for $h_0 h/\mathscr{H}_\rho \ll 1$. At this stage, the current has thinned sufficiently to be modelled as incompressible and the particle-settling shallow-water model of Bonnecaze *et al.* (1993) fully describes the dynamics.

4.1. *Box-model formulation*

We construct a box model of the flow to elucidate the effects of particle settling. The basis of the model is that the evolution of the current is assumed to occur through a series of rectangles containing a constant mass of gas (neglecting entrainment) and a uniform distribution of particles. The total mass of the current decreases as particles settle from the current. This horizontally averaged model gives the correct qualitative behaviour and dependence on parameters, while having the advantage of being simple to formulate. We compare our box-model results with our shallow-water numerical results to show that the simplified model is sufficient for our purposes.

The variables in this section are non-dimensionalized in the same manner as in § 3.3, with densities non-dimensionalized by the initial density $\rho_{i0} = \rho_{gi}/(1-\phi_0)$ at the top of the current, corresponding to the initial particle mass fraction ϕ_0. Recall that the gas density ρ_{gi} at the top of the current is constant under the assumption that p_a is uniform over the height scales considered. Furthermore, in this section we assume that the ambient density is equal to the gas density at the top of the current.

The flow to be described by the box model results from the release of an initially stationary mass of a dense gas–particle mixture, which we take initially to have the same length and height. The constant (dimensionless) mass of gas is given by

$$m_g = x_F \int_0^h \rho_g \, \mathrm{d}z = x_F \bar{\rho}_g h, \tag{4.1}$$

where the height-averaged gas density is given by

$$\bar{\rho}_g = \frac{(1-\phi)\chi}{h}\left[(1 + h_0 h/\mathscr{H})^{c_p/[R(1-\phi)]} - 1\right]; \tag{4.2}$$

$\chi = \mathscr{H} R(1-\phi_0)/(h_0 c_p)$ is a constant and we have expressed γ in terms of $\phi(t)$ with

$c_{pm} = c_p$. We obtain the constant m_g using the initial parameters of the current,

$$x_F(t=0) = 1, \quad h(t=0) = 1 \quad \text{and} \quad \phi(t=0) = \phi_0, \tag{4.3}$$

and use (4.1) to express the height of the current in terms of its length and mass fraction.

Two first-order differential equations describe the evolution of the current. The first equation is the particle-evolution equation. The particle mass fraction $\phi(t)$, which is well-mixed in the current, varies in time due to gravitational particle settling. We neglect particle entrainment into the current. As in the analysis of Bonnecaze *et al.* (1993), we assume that the particles settle out through a small viscous sub-layer at the base of the current where the turbulent gas velocities are diminished to such an extent that the particles leave the base of the current with a flux $v_s\phi$, where v_s is the settling speed. This is an appropriate assumption for dilute particle concentrations where particle–particle interactions may be neglected. We assume that the current has a monodisperse system of particles with the same settling speeds; the box model could be modified to account for a distribution of particle-settling speeds (Dade & Huppert 1996). The conservation law for the particles is given by (Martin & Nokes 1988)

$$\frac{\mathrm{d}\phi}{\mathrm{d}t} = -\frac{\phi\beta}{h}, \tag{4.4}$$

where the settling number $\beta = v_s/(gh_0)^{1/2}$ is a non-dimensional settling velocity. Hence, the rate of decrease of the mass fraction of particles in the current increases as the height $h(t)$ of the current decreases. This model, as well as one which incorporates the advection of particles by the mean flow, has been used successfully in incompressible shallow-water and box models of turbulent, particle-laden flows (Huppert 1998, 2000).

To obtain the second equation, we assume that gravitational collapse is controlled at the head of the current. Hence, from the front condition (3.10), where u is now expressed as $\mathrm{d}x_F/\mathrm{d}t$, we obtain

$$\frac{\mathrm{d}x_F}{\mathrm{d}t} = Fr\sqrt{h\left(1 - \frac{(1-\phi_0)}{\bar{\rho}}\right)}, \tag{4.5}$$

where $\bar{\rho} = \bar{\rho}_g/(1-\phi)$.

4.2. *Box-model solutions*

In the incompressible limit $h_0/\mathscr{H}_\rho \to 0$, there is an analytical solution for the final run-out length of the current, at which point $\phi = 0$. There is no such analytical solution in the compressible case.

We note that in the limiting cases $h_0 h/\mathscr{H}_\rho \ll 1$ and $hh_0/\mathscr{H}_\rho \gg 1$, for a fixed particle mass fraction such that $\gamma - 1 = O(1)$ and $\bar{\rho} \gg \rho_a$, the box model (4.1)–(4.5) yields the same forms, as it must, as the similarity solutions valid in those limits. Solutions to the box model in these limits for a non-settling current are given by

$$h_0 h/\mathscr{H}_\rho \gg 1: \quad x_F(t) = \left(Fr^{2\gamma}\tilde{m}^{\gamma-1}\left(\frac{3\gamma-1}{2\gamma}\right)^{2\gamma}\right)^{1/(3\gamma-1)} t^{2\gamma/(3\gamma-1)}, \tag{4.6}$$

$$h_0 h/\mathscr{H}_\rho \ll 1: \quad x_F(t) = (\tfrac{9}{4}Fr^2 x_0)^{1/3} t^{2/3}, \tag{4.7}$$

where $\tilde{m} = m[\gamma/(\gamma-1)](\mathscr{H}/h_0)^{1/(\gamma-1)}$. These solutions only differ from the shallow-water similarity solutions in the multiplicative constants.

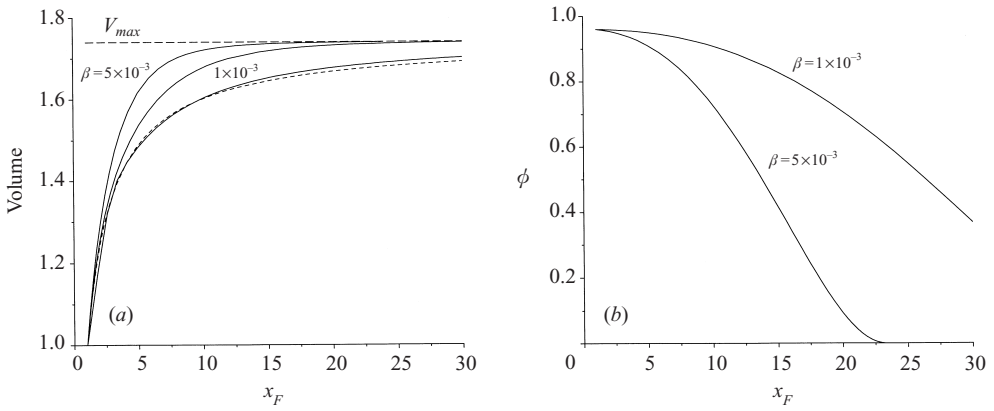

FIGURE 10. (*a*) The volume determined by the box model as a function of x_F for currents with $h_0/\mathscr{H} = 0.012$ and $\phi_0 = 0.96$, having different settling numbers β. The corresponding results of the full shallow-water model, with $\beta = 0$, (the dashed curve) are also shown. (*b*) ϕ as a function of x_F for the currents in (*a*).

Numerical solutions to (4.1)–(4.5) are shown in figure 10. The volume and mass fraction are plotted as a function of x_F for currents with two different settling numbers. The corresponding results of the shallow-water model ($\beta = 0$) indicate that the box model (with $\beta = 0$) yields predictions that agree with our numerical results from the full shallow-water model. Figure 10(*a*) shows that faster particle settling speeds result in a more rapid decompression. During the volume expansion, the density decreases rapidly for only small decreases in ϕ from the initially large mass fraction (cf. figure 3). At long times, the volume asymptotes to the same maximum value V_{max} for both settling and non-settling currents, independent of the value of β. The current attains a (dimensionless) maximum volume given by

$$V_{max} = \frac{m_g}{\lim\limits_{h\to 0} \bar{\rho}_g} = \frac{m_g}{(1-\phi_0)}. \tag{4.8}$$

While sedimentation plays an important role in the rate of decompression of the mixture, figure 10(*b*) shows that only a small fraction of the particles leaves the current during the decompression phase, since the scale height increases rapidly as ϕ decreases from values very close to 1 (figure 2). The majority of settling occurs after the current achieves an essentially constant volume, which is an even more rapid process for a settling current. Bonnecaze *et al.* (1993) incorporated particle settling into their shallow-water model of an incompressible current and showed that there is no significant effect of particle settling on the flow dynamics before the current evolves to its self-similar form given by (3.22).

Figure 11 compares the length as a function of time for the current in figure 10, with no settling and for two different settling numbers. At early times, the lengths of the settling currents are the same as the lengths of the non-settling currents. At later times, the lengths of the settling currents become less because of the reduction in the buoyancy driving force with mass loss through sedimentation.

5. Conclusions

We have demonstrated the important effects of compressibility in gas–particle gravity currents in which the flow thickness is comparable in magnitude to the

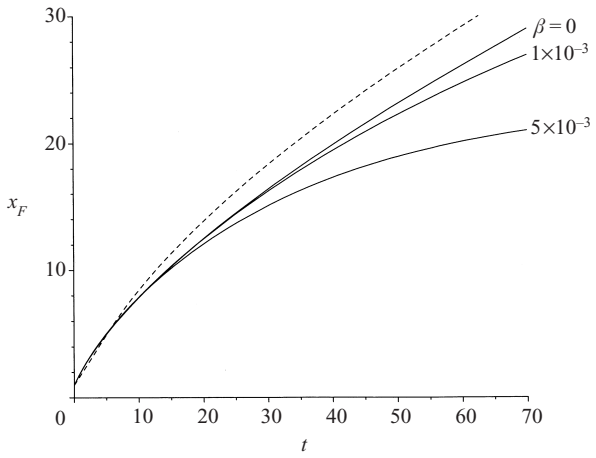

FIGURE 11. x_F as a function of time for the current in figure 10, determined by the box model. The corresponding results of the full shallow-water model ($\beta = 0$) are shown by the dashed curve.

density scale height of the flow. The presence of particles in the gas can greatly reduce the scale height by having a significant effect on the bulk density without significantly reducing the compressibility. Hence, we have incorporated a pressure-dependent density into shallow-water and box models of the flow, including the contribution of particles to the density and thermodynamics.

We have shown that the shallow-water equations, together with the front condition, for a compressible current with constant particle mass fraction admit similarity solutions in the two limits of a very large current thickness relative to its density scale height and vice versa. We have numerically solved the shallow-water equations for the case of no particle settling and verified the similarity solutions by the numerical results. The main feature of compressible currents that distinguishes them from incompressible currents is that the mixture decompresses upon gravitational collapse. As a result, these flows travel faster than their incompressible counterparts because the internal energy of compression, together with some buffering thermal energy from the particles, becomes available upon decompression to be transformed into kinetic energy of motion. The effects of compressibility decrease as the current spreads and thins, and can be ignored after the height of the current becomes much less than the density scale height of the mixture.

We have formulated a box model, in which we assume that there is no horizontal variation of properties in the flow, to capture the essential features of particle settling during the decompression phase of a particle-laden flow. The box model gives a good indication of the shallow-water model results for a non-settling current. We show that only a very small fraction of particles settles out of the current during the decompression phase because the small mass loss leads to a rapid decompression. Compressibility is thus most important in the initial stages and proximal region of a pyroclastic flow, and serves to establish a connection between the dense eruption conditions and the more distal behaviour, which can be modelled by simpler incompressible models. The extent of compressible effects depends chiefly on h_0 and ϕ (figure 2).

The volume expansion and faster propagation speeds have important implications for the interactions of compressible flows with regional topography, for example, ridges and mountains. At the larger volumes and speeds, particle-driven gravity

currents can pass over higher topographic barriers, so that the potential devastation zone becomes greater. Moreover, hazard assessment becomes more difficult because decompression results in velocities larger than those of an incompressible current, putting larger areas at risk.

Application to Martian dust storms must be more speculative since *in situ* observations are not available. Nevertheless, we note that, because of the free upper surface, these compressible currents do not support gas dynamic shocks. Though the flow velocities can be greater than the sound speed in the mixture, it is unhelpful to think of analogies to supersonic flow, since the pressure distribution remains hydrostatic. Instead, we note that these gravity currents, like all gravity currents, support hydraulic jumps both within the current and at the front. The mechanism of particle entrainment and self-ignition for Martian dust storms, as invoked by Parsons (2000), may thus be related to these hydraulic jumps rather than to compressible shocks.

In order to focus on developing a description of the effects of compressibility in a particle-driven gravity current, we have focused on the simplest case, namely one-dimensional propagation of a finite-volume monodisperse release on a horizontal plane. It is straightforward to adapt this description for the cases of continual release, axisymmetric spread, polydispersity and flow on a slope (Bonnecaze *et al.* 1995; Bonnecaze, Huppert & Lister 1996; Bonnecaze & Lister 1999). Axisymmetric currents will, of course, decompress more rapidly owing to the geometrical spreading. The assumption of complete vertical mixing of particles, momentum and entropy could be relaxed at the expense of introducing a closure model for the suppression of turbulence by internal stratification (Parker, Fukushima & Pantin 1986). Re-entrainment of particles might be possible in some circumstances, with the modelling of turbulent pick-up rates also relying on a semi-empirical approach. In each of these more complicated extensions to our work, the dynamical significance of compressibility, the reduction of the density scale height by particle loading, and the ratio of the height of the current to the density scale height are expected to carry over from the simple case.

Appendix. Numerical method

We solved the shallow-water equations numerically by adapting the numerical scheme of Bonnecaze *et al.* (1993) to include the effects of compressibility. This scheme is based on the two-stage Lax–Wendroff scheme, which is explicit and second order in both time and space. A small nonlinear dissipation term is introduced to suppress spurious oscillations near shocks. While the evolution of the interior points is fully specified in the two-stage Lax–Wendroff scheme, there are problems at the boundaries. To obtain a unique solution, we need to specify u and h at each boundary. We have two boundary conditions, one at the front and the other at the tail, while we must determine four variables and hence we need two more conditions at the boundaries. For this hyperbolic system of equations, the number and location of the specified boundary conditions are the same as the number and location of the characteristics that propagate into the flow domain. We derive the additional conditions at the boundaries from the characteristic equations that hold along the characteristics which propagate out of the flow domain.

We introduce the conservative variable $l = \bar{\rho}h$ to express (3.11) and (3.12) in matrix form as

$$\frac{\partial}{\partial t}\begin{pmatrix} l \\ u \end{pmatrix} + \begin{pmatrix} u & l \\ a^2/l & u \end{pmatrix}\frac{\partial}{\partial x}\begin{pmatrix} l \\ u \end{pmatrix} = \begin{pmatrix} 0 \\ 0 \end{pmatrix}, \tag{A 1}$$

where

$$l = \frac{\gamma - 1}{\gamma}\frac{\mathscr{H}}{h_0}\left[\left(1 + \frac{h_0 h}{\mathscr{H}}\right)^{\gamma/(\gamma-1)} - 1\right], \tag{A 2}$$

$$a^2 = l\left(1 + \frac{hh_0}{\mathscr{H}}\right)\left(1 + \frac{\gamma}{\gamma - 1}\frac{lh_0}{\mathscr{H}}\right)^{-1}. \tag{A 3}$$

The eigenvalues of the coefficient matrix in (A 1) give the two characteristic velocities in the flow, $u \pm a$, corresponding to the forward and backward propagating wave speeds for shallow-water waves. Using the corresponding right eigenvectors $(\pm a/l, 1)$ of the coefficient matrix, we deduce the relationships between the variables on the characteristics

$$\mathrm{d}u \pm \frac{a}{l}\,\mathrm{d}l = 0 \quad \text{on} \quad \left(\frac{\mathrm{d}x}{\mathrm{d}t}\right)_{\pm} = u \pm a. \tag{A 4}$$

Hence, with the boundary conditions, we have two equations and two unknowns on each boundary.

The front of the current is a moving boundary and, following Bonnecaze *et al.* (1993), it is convenient to transform the governing equations from the (x, t) coordinate system to a (y, τ) coordinate system where $y = x/x_F(t)$ and $\tau = t$, so that the new spatial coordinate y lies between 0 and 1; the front of the current is at the fixed point $y = 1$. The differentials are given by

$$\frac{\partial}{\partial t} = \frac{\partial}{\partial \tau} - y\frac{\dot{x}_F}{x_F}\frac{\partial}{\partial y} \quad \text{and} \quad \frac{\partial}{\partial x} = \frac{1}{x_F}\frac{\partial}{\partial y}, \tag{A 5}$$

where $\dot{x}_F = \mathrm{d}x_F/\mathrm{d}t$. We apply these differential transforms to (A 1) and introduce another conservative variable, $q = \bar{\rho}uh$, to obtain

$$\left.\begin{aligned} \frac{\partial l}{\partial t} &= \frac{1}{x_F}\left(y\dot{x}_F\frac{\partial l}{\partial y} - \frac{\partial q}{\partial y}\right), \\ \frac{\partial q}{\partial t} &= \frac{1}{x_F}\left(y\dot{x}_F\frac{\partial q}{\partial y} - \frac{\partial}{\partial y}\left[\frac{q^2}{l} + \frac{\gamma - 1}{2\gamma - 1}\left(l\frac{\mathscr{H}}{h_0}(1 + h_0 h/\mathscr{H}) - \frac{h\mathscr{H}}{h_0}\right)\right]\right), \end{aligned}\right\} \tag{A 6}$$

where we have replaced τ by t. Finally, the characteristic equations satisfied along characteristics that propagate out of the flow domain are given by

$$\left.\begin{aligned} \mathrm{d}u - \frac{a}{l}\,\mathrm{d}l = 0 \quad &\text{on} \quad \frac{\mathrm{d}y}{\mathrm{d}t} = \frac{1}{x_F}(u - y\dot{x}_F - a), \\ u = 0 \quad &\text{at} \quad y = 0, \end{aligned}\right\} \tag{A 7}$$

and

$$\left.\begin{aligned} \mathrm{d}u + \frac{a}{l}\,\mathrm{d}l = 0 \quad &\text{on} \quad \frac{\mathrm{d}y}{\mathrm{d}t} = \frac{1}{x_F}(u - y\dot{x}_F + a), \\ u = Fr\sqrt{h} \quad &\text{at} \quad y = 1, \end{aligned}\right\} \tag{A 8}$$

where we have also restated the boundary conditions.

The numerical scheme was verified by comparisons of the height and velocity profiles with previous incompressible calculations and with the similarity solutions, and by the usual checks of robustness with respect to variations of time step and grid spacing.

REFERENCES

Benjamin, T. 1968 Gravity currents and related phenomena. *J. Fluid Mech.* **31**, 209–248.

Bohren, C. & Albrecht, B. 1998 *Atmospheric Thermodynamics*. Oxford University Press.

Bonnecaze, R., Hallworth, M., Huppert, H. & Lister, J. 1995 Axisymmetric particle-driven gravity currents. *J. Fluid Mech.* **294**, 93–121.

Bonnecaze, R., Huppert, H. & Lister, J. 1993 Particle-driven gravity currents. *J. Fluid Mech.* **250**, 339–369.

Bonnecaze, R., Huppert, H. & Lister, J. 1996 Patterns of sedimentation from polydispersed turbidity currents. *Proc. R. Soc. Lond.* A **452**, 2247–2261.

Bonnecaze, R. & Lister, J. 1999 Dynamics and deposition of particle-driven gravity currents down slopes. *J. Fluid Mech.* **390**, 75–91.

Dade, W. & Huppert, H. 1996 Emplacement of the Taupo ignimbrite by a dilute turbulent flow. *Nature* **381**, 509–512.

Dobran, F. & Neri, A. 1993 Numerical simulation of collapsing volcanic columns. *J. Geophys. Res.* **98**, 4231–4259.

Gill, A. 1982 *Atmosphere-ocean dynamics*. Academic Press.

Grobelbauer, H., Fannelop, T. & Britter, R. 1993 The propagation of intrusion fronts of high density ratios. *J. Fluid Mech.* **250**, 669–687.

Huppert, H. 1998 Quantitative modelling of granular suspension flows. *Phil. Trans. R. Soc. Lond.* A **356**, 2471–2496.

Huppert, H. 2000 Geological fluid mechanics. In *Developments in Fluid Mechanics for the Millennium. A Collective Introduction to Current Research* (ed. G. Batchelor, H. Moffatt & M. Worster), pp. 447–495. Cambridge University Press.

Huppert, H. & Simpson, J. 1980 The slumping of gravity currents. *J. Fluid Mech.* **99**, 785–799.

Kármán, T, von 1940 The engineer grapples with nonlinear problems. *Bull. Am. Math. Soc.* **46**, 615–683.

Kieffer, S. 1984 Laboratory studies of volcanic jets. *J. Geophys. Res.* **89 B10**, 8253–8268.

Klemp, J. B., Rotunno, R. & Skamarock, W. 1994 On the dynamics of gravity currents in a channel. *J. Fluid Mech.* **269**, 169–198.

Martin, D. & Nokes, R. 1988 Crystal settling in a vigorously convecting magma chamber. *Nature* **332**, 534–536.

Neri, A. & Macedonio, G. 1996 Numerical simulation of collapsing volcanic columns with particles of two sizes. *J. Geophys. Res.* **101**, 8153–8174.

Parker, G., Fukushima, Y. & Pantin, H. 1986 Self-accelerating gravity currents. *J. Fluid Mech.* **171**, 145–181.

Parsons, J. 2000 Are fast-growing Martian dust storms compressible? *Geophys. Res. Lett.* **27**, 2345–2348.

Simpson, J. 1987 *Gravity Currents in the Environment and the Laboratory*. John Wiley and Sons.

Sparks, R., Bursik, M., Carey, S., Gilbert, J., Glaze, L., Sigurdsson, H. & Woods, A. 1997 *Volcanic Plumes*. John Wiley and Sons.

Valentine, G. & Wohletz, K. 1989 Numerical models of plinian eruption columns and pyroclastic flows. *J. Geophys. Res.* **94** (B2), 1867–1887.

Wallis, G. 1969 *One-Dimensional Two-Phase Flow*. McGraw-Hill.

Wood, S. & Battino, R. 1990 *Thermodynamics of Chemical Systems*. Cambridge University Press.

Woods, A. 1988 The fluid dynamics and thermodynamics of eruption columns. *Bull. Volcanol.* **50**, 169–193.

Woods, A. 1995 The dynamics of explosive volcanic eruptions. *Rev. Geophys.* **33**, 495–530.